PeptideScience
THE AMERICAN PEPTIDE SOCIETY JOURNAL

Special Issue: Materials and Applications

Guest Editor: Jean Chmielewski (Purdue University)

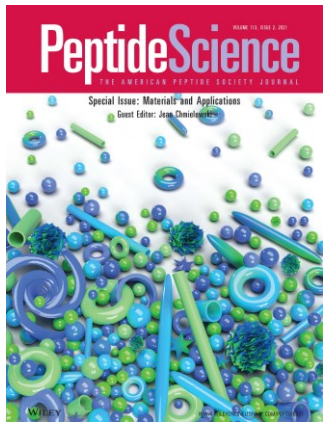

EDITORIAL

Emerging designs and applications of peptide-based materials
Jean Chmielewski, *Peptide Science* 2021, doi: 10.1002/pep2.24226

REVIEWS

A comparison of the collagen triple helix and coiled-coil peptide building blocks on metal ion-mediated supramolecular assembly
Ryan W. Curtis and Jean Chmielewski, *Peptide Science* 2021, doi: 10.1002/pep2.24190

Fluorinated peptide biomaterials
Janna N. Sloand, Michael A. Miller and Scott H. Medina, *Peptide Science* 2021, doi: 10.1002/pep2.24184

Multivalent display of chemical signals on self-assembled peptide scaffolds
Hannah E. Distaffen, Christopher W. Jones, Brittany L. Abraham and Bradley L. Nilsson, *Peptide Science* 2021, doi: 10.1002/pep2.24224

Peptides as key components in the design of non-viral vectors for gene delivery
Joseph Thomas, Kamia Punia and Jin Kim Montclare, *Peptide Science* 2021, doi: 10.1002/pep2.24189

Cyclic dipeptides: Biological activities and self-assembled materials
Kaili Zhao, Ruirui Xing and Xuehai Yan, *Peptide Science* 2021, doi: 10.1002/pep2.24202

Dual-peptide functionalized nanoparticles for therapeutic use
Chelsea R. Forest, Caitlin A. C. Silva and Pall Thordarson, *Peptide Science* 2021, doi: 10.1002/pep2.24205

Capturing nested information from disordered peptide phases
Christella K. Gordon, Regina Luu and David Lynn, *Peptide Science* 2021, doi: 10.1002/pep2.24215

ARTICLES

Enzymatically forming cell compatible supramolecular assemblies of tryptophan-rich short peptides
Dongsik Yang, Beom Jin Kim, Hongjian He and Bing Xu, *Peptide Science* 2021, doi: 10.1002/pep2.24173

Short self-assembling peptides with a urea bond: A new type of supramolecular peptide hydrogel materials
Hiroshi Tsutsumi, Kunifumi Tanaka, Jyh Yea Chia and Hisakazu Mihara, *Peptide Science* 2021, doi: 10.1002/pep2.24214

Functionalized peptide hydrogels as tunable extracellular matrix mimics for biological applications
Katharina S. Hellmund, Benjamin von Lospichl, Christoph Böttcher, Kai Ludwig, Uwe Keiderling, Laurence Noirez, Annika Weiß, Dorian J. Mikolajczak, Michael Gradzielski and Beate Koksch, *Peptide Science* 2021, doi: 10.1002/pep2.24201

PeptideScience
THE AMERICAN PEPTIDE SOCIETY JOURNAL

Special Issue: Materials and Applications

Guest Editor: Jean Chmielewski (Purdue University)

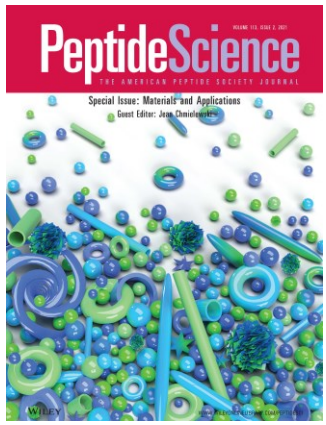

Received: 1 July 2020 | Revised: 8 September 2020 | Accepted: 23 September 2020

DOI: 10.1002/pep2.24201

ARTICLE

PeptideScience WILEY

Functionalized peptide hydrogels as tunable extracellular matrix mimics for biological applications

Katharina S. Hellmund[1] | Benjamin von Lospichl[2] | Christoph Böttcher[3] | Kai Ludwig[3] | Uwe Keiderling[4] | Laurence Noirez[5] | Annika Weiß[1] | Dorian J. Mikolajczak[1] | Michael Gradzielski[2] | Beate Koksch[1]

[1]Department of Biology, Chemistry, Pharmacy, Institute of Chemistry and Biochemistry–Organic Chemistry, Freie Universität Berlin, Berlin, Germany

[2]Stranski-Laboratory of Physical and Theoretical Chemistry, Institute of Chemistry, Technische Universität Berlin, Berlin, Germany

[3]Center of Electron Microscopy at Freie Universität Berlin, Institute of Chemistry and Biochemistry and CoreFacility BioSupraMol Freie Universität Berlin, Berlin, Germany

[4]Department Experiment Control and Data Acquisition, Helmholtz-Zentrum Berlin für Materialien und Energie, Berlin, Germany

[5]Laboratoire Léon Brillouin (CEA-CNRS) Université Paris-Saclay, Gif-sur-Yvette Cédex, France

Correspondence
Beate Koksch, Institute of Chemistry and Biochemistry–Organic Chemistry, Freie Universität Berlin, Arnimallee 20, 14195 Berlin, Germany.
Email: beate.koksch@fu-berlin.de

Funding information
DFG-CRC 765 Multivalency, Grant/Award Number: SFB 765/2-2014

Abstract

The development of tailorable and biocompatible three-dimensional (3D) substrates or molecular networks that reliably mimic the extracellular matrix (ECM) and influence cell behavior and growth *in vitro* is of increasing interest for cell-based applications in the field of tissue engineering and regenerative medicine. In this context, we present a novel coiled coil-based peptide that self-assembles into a 3D-α-helical fibril network and functions as a self-supporting hydrogel. By functionalizing distinct coiled-coil peptides with cellular binding motifs or carbohydrate ligands (mannose), and by utilizing the multivalency and modularity of coiled-coil assemblies, tailored artificial ECMs are obtained. Fibrillar network and ligand density, as well as ligand composition can readily be adjusted by changes in water content or peptide concentrations, respectively. Mesoscopic structure of these networks was assessed by rheology and small-angle neutron scattering experiments. Initial cell viability studies using NIH/3T3 cells showed comparable or even superior cell viability using the presented artificial ECMs, compared to commercially available 3D-cell culture scaffold Matrigel. The herein reported approach presents a reliable (low batch-to-batch variation) and modular pathway toward biocompatible and tailored artificial ECMs.

KEYWORDS
coiled coil, extracellular matrix, peptide hydrogel, SANS

1 | INTRODUCTION

Extracellular matrices (ECM) are complex three-dimensional (3D) networks of macromolecules that play a pivotal role in processes that direct cell fate and behavior *in vivo*.[1–5] ECMs typically comprise various proteins, including laminin, collagens, elastin, proteoglycans, and an intricate mixture of growth factors, adhesion ligands and other soluble molecules.[6] The sophisticated molecular environment that is generated by the ECM provides and supports important cellular functions, such as growth, maintenance, and differentiation of various cells. Therefore, the development of synthetic materials that closely resemble the environment of natural ECM, to enable increased cell viability, proliferation and tissue specific differentiation *in vitro* is of increasing interest for medical and clinical applications and tissue engineering.

Various *in vitro* growth materials have been developed based on hydrogels of different polymers or cross-linked carbohydrates.[7] However, the hydrogel formulation of these materials is not applicable to all cell types. Therefore, natural ECM extracts from living cells are widely utilized as they contain advantageous mixtures of structural proteins and growth factors for more sensitive cell-growth

conditions.[1] One of the most applied cell culture extracts is commercialized as Matrigel (BD Biosciences, Mississauga, Canada).[8,9] Albeit, the established success of such extracts from cells as 3D-cell culture matrices, individual extraction batches possess ill-defined compositions and quantities of individual components, which affects experimental performance.[10,11] Moreover, tuning of mechanical or biochemical properties entails the risk for contamination or degradation.[10] Thus, one of our main research goals in this field, which we see as a complementary approach to cell extracts, is the development of a synthetic 3D-cell-culture matrix, which is inherently modular and allows for the presentation of defined amounts of desired (biochemical) ligands, while mechanical properties can readily be fine-tuned.

Chemically synthesized peptide-based materials may present a pathway toward such 3D-matrices. Designed peptides possess the ability to adopt well-defined secondary, tertiary or even higher-ordered quaternary structures and assemble into complex 3D-architectures. The molecular complexity of peptidic structures can be fine-tuned by changes in the primary structure and incorporation of, for example, non-canonical amino acid building blocks,[12] or by introduction of small molecule ligands or glycans into specific amino acid side chains.[13,14] Peptides can be synthesized with a low batch-to-batch variation in high purity using solid-phase-peptide-synthesis (SPPS) and their folding behavior into the programmed structures is reliably and reproducible. In fact, prior studies from our group have demonstrated that these sytems are robust enough to provide for the functional display of a covalently linked sugar moiety or peptide epitope. In particular, it was shown that a galactose moiety is displayed to asialoglycoprotein receptors on HepG2 cells, enabling the specific ASGPR-mediated uptake of the peptides into cells (this was not found to be the case in nonexpressing negative control cell lines HeLa and L929).[14] In the other study, we showed that the solvent-accessibility or display of the Ep01 peptide on this type of fiber-forming peptidic system enabled antidiphtheria toxin antibody binding, as well as lectin binding and bacterial cell binding to a displayed mannose sugar.[13] The potential of peptides to function as 3D-cell culture substrates has already been successfully proven.[15]

Among the plethora of available peptide structures, the α-helical coiled-coil motif is a well-characterized naturally occurring folding motif commonly used in various peptidic model systems.[16] The coiled-coil motif consists of two to seven α-helices that wrap around each other to form a left-handed superhelical twist.[16,17] The primary amino acid sequence is characterized by a repetition of seven amino acids, called heptad repeat.[16] Amino acids within a heptad repeat are denoted as *a-b-c-d-e-f-g*, where positions *a* and *d* are commonly occupied by nonpolar amino acid residues, such as leucine, isoleucine, and valine, which form the hydrophobic core of the helix bundle[18,19] that directs the folding and packing of the amphipathic structure.[16] Positions *e* and *g* are occupied mostly by charged amino acids like arginine, glutamic acid and lysine that provide intermolecular ionic interactions between the individual peptide helices and direct orientation of the coiled coil.[17,20] The remaining positions *b*, *c* and *f* are located at the solvent-exposed region at the periphery of the α-helices and are appropriate positions for side chain modifications with, for example, carbohydrate moieties or peptide ligands.[13,14,17] Individual coiled-coil peptide sequences can be functionalized with diverse ligands, enabling the generation of customized peptide monomers that afterwards assemble into tailored coiled-coil structures. Studies by Hodges *et al*., Kim *et al*. and Woolfson *et al*., established rules for the design of α-helical peptide bundles with a predictable degree of oligomerization,[21–25] further extending the design scope of these structures. The coiled-coil folding motif has proven to be an advantageous and reliable platform for the generation of many biomaterials that find application in, for example, tissue engineering[26–29] or as versatile substrates for cell culture experiments.[15]

Woolfson and coworkers showed that a heterodimeric coiled coil-based hydrogel (hSAFs), which includes more than 99% water (by weight), supports the growth and differentiation of PC12 cells, however, to a lesser extent than the control substrate Matrigel.[30] The overall lower growth was associated with the absence of cell-recognition motifs, or growth factors, which are present within Matrigel.

Another study by Woolfson and coworkers, reported that the same heterodimeric coiled coil-based self-organizing hSAFs hydrogels, which have been additionally decorated with the RGDS tetrapeptide, a recognition motif from fibronectin,[31] form 3D biomaterials that are able to increase the proliferative activity of embryonic neuronal stem cells (NSCs), thus, support the differentiation of NSCs.[28] This example also highlights the potential of coiled-coil-based 3D-substrates also for stem cell culture.

To tie in with the given background, we designed a peptide sequence, namely hFF03 (Table 1) that consist of only four different amino acids and is based on a homomeric coiled-coil dimer. hFF03 self-assembles into stable α-helical fibers and builds up self-supporting hydrogels under physiological conditions as well as enables the presentation of biologically relevant ligands at the same time. Thus, hFF03 was modified with the tripeptide ligand, RGD, as well as with the monosaccharide mannose resulting in three hFF03 variants that can be combined at will to generate tailored artificial ECM. Conjugation of these molecules was achieved by using a previously reported all-on-solid-phase approach, where RGD-sequence and mannose were included by standard solid phase peptide synthesis (Figure 1).[13]

The presented rational design approach utilizes the modularity of the coiled-coil system to enable a systematic study of the structure and stability of hydrogel formation depending on the nature and concentration of a recognition motif (RGD) or carbohydrate ligand (mannose) as well as the combination of both, bound to one 3D scaffold. In the following, hFF03 and its variants are systematically studied, in terms of peptide secondary structure, mechanical properties and cytotoxicity, as pure compounds and as mixtures, in various compositions and concentrations (Table S1).

TABLE 1 Synthesized peptide hFF03 and its modified variants

	Sequence/ligand
hFF03	LKKELAALKKELAALK**K**ELAALKKEL
hFF03-K17-Man	LKKELAALKKELAALK**K(Man)**ELAALKKEL
hFF03-K17-RGD	LKKELAALKKELAALK**K(RGD)**ELAALKKEL

Note: Bold K represents ligand bearing position.

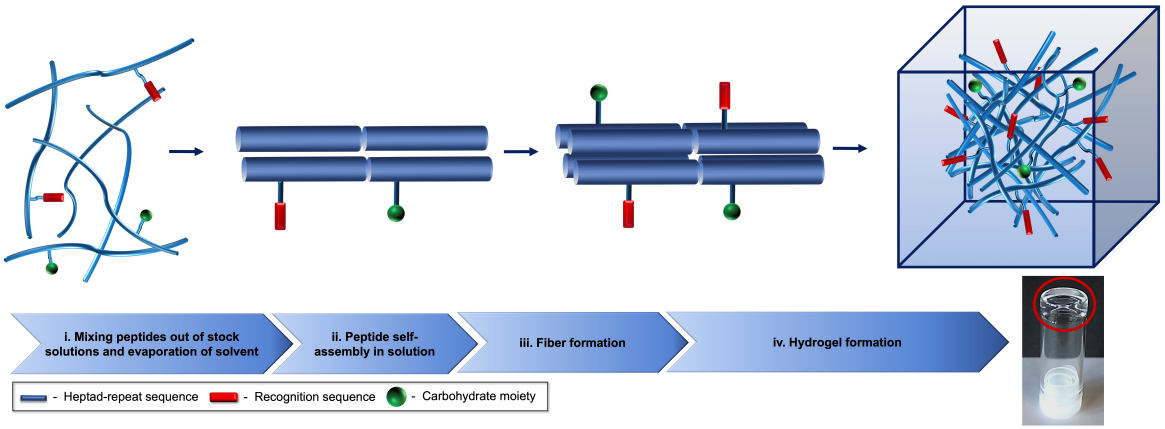

FIGURE 1 Schematic representation of hydrogel formation by mixing of different ligand presenting coiled coil peptides. Hydrogel formation indicated by inversion of the sample vial (bottom right)[32]

2 | MATERIALS AND METHODS

2.1 | Peptide synthesis

Solid-phase peptide synthesis was performed on resins acquired from Novabiochem. All Fmoc-protected amino acids were purchased from Orpegen. hFF03 and hFF03 variants were synthesized using preloaded Fmoc-Leu-NovaSyn TGA resin (0.2 mmol/g substitution), respectively. Synthesis was performed by standard Fluorenylmethyloxycarbonyl-(Fmoc)-chemistry on a 0.1 mmol scale. Fmoc-deprotection was performed with 2% piperidine and 2% 1,8-Diazabicyclo[5.4.0]undec-7-en in DMF (3 × 7 min using 5 mL of deprotecting solution) at each step.

Synthesis of hFF03 and hFF03-variants was accomplished in two steps: hFF03 was synthesized by performing two coupling steps per amino acid (1 hour each coupling) using an automated synthesizer Activo P-11 Automated Peptide Synthesizer (Activotec, Cambridge, United Kingdom) and amino acid (8 eq.), 2-(1H-7-Azabenzotriazol-1-yl)-1,1,3,3-tetramethyluronoium hexafluorphosphate (HATU, 8 eq.), as well as *N*,*N*-diisopropylethylamin (DIPEA, 16 eq.) relative to resin loading. In case of decorated variants of hFF03 tBu-protected lysine in position 17 was substituted for *N*-Methyltrityl-protected (Mtt) lysine purchased from Carbolution. After full-length synthesis of the peptides, Boc-aminobenzoic acid (Abz; Bachem, Bachem AG; Bubendorf, Switzerland) was coupled to the *N*-terminus of each hFF03 variant as a chromophore. Further synthesis of hFF03-variants was performed by selective deprotection of lysine (Mtt) side chain by treatment with a solution containing 1% TFA (vol/vol) and 1% MeOH (vol/vol) in DCM according to the literature established protocols.[33] The free amine group of lysine 17 side chain is used as starting point for further coupling of either RGD or mannose.

In case of the tripeptide RGD, manual SPPS was performed using the respective amino acid (8 eq.), HATU (8 eq.) and DIPEA (16 eq.) relative to resin loading. Fmoc-deprotection was performed at each step as described above.

In case of mannose-functionalization, amino functionality was converted into a carboxy-functionality by addition of a mixture of glutaric anhydride (3 eq.) and catalytic amounts of DIPEA. The syringe was shaken for 3 hours. Afterward carboxy function was activated using (1-Cyano-2-ethoxy-2-oxoethylidenaminooxy)dimethylamino-morpholino-carbenium hexafluoro-phosphate (3. eq.) and DIPEA (6 eq.). Immediately after, 1-amino-1-deoxy-mannopyranose (Santa Cruz) was coupled to carboxy function.

Full cleavage of all peptides from resin was performed by addition of 10 mL of a cleavage cocktail containing 95% TFA, 3% H_2O and 2% Triisopropylsilane to the corresponding syringe followed by 3.5 hours of agitation. Peptides were precipitated using ice cold diethylether. After decantation of ether, peptides were redissolved in water and lyophilized. Purification of peptides was achieved using preparative HPLC.

2.2 | Exchange of TFA adduct

TFA adducts inevitably obtained during full cleavage of peptides from resin using TFA and subsequent RP-HPLC purification using eluents containing 0.1% TFA, was exchanged against chloride according to the established literature protocols.[34] Briefly, peptides were dissolved in water at a concentration of 0.52 mM. Afterward 6 M HCl was mixed to peptide solutions to give final concentration of 7.5 mM HCl. The solutions were stirred at room temperature for 1 minute prior to lyophilization. This procedure was repeated five times.

2.3 | Dialysis of peptides

Dialysis of peptides was performed by using Spectra/Por Float-A-Lyzer (Carl Roth) with molecular weight cutoff of 100 to 500 Da according to suppliers' instructions. Peptides were dialyzed against deionized water over 3 days. Water was changed three times a day. After completion, peptide solutions were lyophilized.

2.4 | Sample preparation

Pure peptides were dissolved in 1 mL 1,1,1,3,3,3-Hexafluoroisopropanol and sonicated for 15 minutes. Peptide concentration was determined by UV-spectroscopy at 320 nm (Abz). An aliquot of the stock solution was briefly evaporated using a stream of N_2-gas and the pellet dissolved in 1 mL of D-PBS containing 6 M of guanidine hydrochloride. Absorbance at 320 nm of this solution was measured using a Varian Cary 50 photometer (Varian Medical Systems, Palo Alto, CA, USA). The concentrations of stock solutions were calculated using a calibration curve of Abz-Gly-OH. For certain peptide concentrations, the required aliquots were completely evaporated and dissolved in buffer solution. In case of hydrogel-mixtures aliquots of desired peptide stock-solutions were mixed before evaporation. After evaporation, peptides were dissolved in dulbeccos phosphate buffered saline (Lonza, w/o Mg^{2+}, Ca^{2+}) or DMEM (Lonza, 4.5 g/L glucose). and pH adjusted to 7.4 using HCl or NaOH.

2.5 | Circular dichroism spectroscopy

Circular dichroism (CD) spectra of peptide hydrogels were recorded using a Quartz Suprasil cuvette with detachable windows and a path length of 0.1 mm (Hellma Analytics, Müllheim, Germany). Measurements were performed at 37 °C. A mean of three independent measurements was performed. CD spectra are background-corrected by subtraction of buffer spectra at 37 °C and spectra were normalized according to the path length of the cuvette, peptide concentration and number of amide-bonds.

2.6 | Cryo-transmission electron microscopy

Cryo-transmission electron microscopy (Cryo-TEM) was measured using 0.15 wt% peptide hydrogel samples. A volume of 5 μL aliquots of the respective peptide gels were applied to pre-cleaned 200 mesh perforated carbon film-covered microscopical grids (R1/4 batch of Quantifoil, MicroTools GmbH, Jena, Germany). The grids were cleaned with chloroform and hydrophilized by 60 seconds glow discharging at 8 W in a BALTEC MED 020 device (Leica Microsystems, Wetzlar, Germany). Vitrifying of the samples occurred by automatic blotting and plunge freezing with a FEI Vitrobot Mark IV (Thermo Fisher Scientific Inc., Waltham, Massachusetts, USA) using liquid ethane as cryogen. The vitrified samples were transferred to the autoloader of a FEI TALOS ARCTICA electron microscope (Thermo Fisher Scientific Inc., Waltham, Massachusetts, USA). The microscope is equipped with a high-brightness field-emission gun (XFEG), which operates at an acceleration voltage of 200 kV. Acquisition of the micrographs was carried out on a FEI Falcon 3 direct electron detector (Thermo Fisher Scientific Inc., Waltham, Massachusetts, USA) using a 70 μm objective aperture at a nominal magnification of 28 000 or 36 000×, corresponding to a calibrated pixel size of 3.69 or 2.97 Å/pixel, respectively.

2.7 | Rheology

All rheological measurements were performed using a temperature-controlled Bohlin Gemini 200 HR Nano rheometer using the strain-imposed mode. The samples were measured at room temperature (25 °C) and at physiological temperature (37 °C). All experiments were conducted using a plate-plate geometry with the upper rotating plate having a diameter of 40 mm. The plates are made of stainless steel. The gap size between the two plates was kept constant at 200 μm. To avoid evaporation effects the setup of sample and confining geometry was surrounded by a solvent trap. For reasons of reproducibility, all rheological experiments were repeated three times. From these triplicate measurements the error bars were estimated and found to be in the range of 10% to 20% of the measured values.

2.8 | Small angle neutron scattering

Small angle neutron scattering (SANS) experiments were performed at the Helmholtz-Zentrum Berlin (HZB, Berlin, Germany) on the instrument V4 and at the Laboratoire Leon Brillouin (LLB, Saclay, France) on the instrument PAXY. For the measurements at V4 (HZB) three different sample-detector-distances D_1 = 1.35 m, D_2 = 6.75 m and D_3 = 16.0 m were used. The wavelength for D_1 and D_2 was set at 4.5 Å, while for D_3 a wavelength of 10.0 Å was used. This enabled covering a q-range of 0.02 to 6.5 nm^{-1}, where $q = 4\pi \sin(\theta/2)/\lambda$ is the scattering vector with θ being the scattering angle. Also for the measurements at PAXY (LLB) three sample-detector-distances D_1 = 1 m, D_2 = 5 m, and D_3 = 6.7 m were used, whereby for D_1 and D_2 the wavelength was set to 4.0 Å and for D_3 to 12.0 Å allowing to cover a q-range of 0.04 to 6.3 nm^{-1} similar to the experiments at V4. To have comparable experimental conditions for all measurements 2 mm Hellma QS 110 cuvettes were used throughout. During the experiments all samples were kept at 25 °C. To reduce the two-dimensional detector images to one-dimensional datasets the BerSANS software[35] was used for the data collected at V4, while for the data recorded at PAXY the PASiNET software[36] was used. For both reduction methods the one-dimensional data were obtained as differential cross sections by taking into account the samples transmission and comparing the scattering intensities to the one of a H_2O sample with 1 mm thickness.

2.9 | Cytotoxicity of different hydrogel compositions

2.9.1 | Cell culture

NIH/3T3 embryonic mouse fibroblast cells were cultured in DMEM culture medium (Lonza, 4,5 g/L glucose, 10% FCS, 1% penicillin/streptomycin) in a humidified incubator (5% CO_2, 37 °C). The cells were grown in 175 cm^2 cell culture flaks and medium was changed three times a week. Upon confluency of 70% to 80% the culture was subcultured according to the detected cell number. The cells were

supported by the research group of Prof. Marie Weinhart (Freie Universität Berlin/Leibniz Universität Hannover). The cells were tested against mycoplasma contamination before use.

2.10 | Cytotoxicity assay of hydrogel cultured NIH/3T3 cells by use of Cell Counting Kit-8

To determine whether different peptide hydrogel compositions would be tolerated by the cells Cell Counting Kit-8 (CCK-8) was used to conduct viability of cells during a 3 days cell culture. A suspension of NIH/3 T3 cells in DMEM (4.5 g/L, 10% FCS, 1% penicillin/streptomycin) was seeded in a transparent 96-well plate with a density of 10 000 cells in an overall volume of 100 μL per well containing the respecting hydrogels. A volume of 10 μL of 1% (wt/vol) SDS was added to the respective wells of positive control and the plate was further incubated for 24 hours and 72 hours at 37 °C and 5% CO_2, respectively. After each time point 10 μL of CCK-8 solution was added to each well and allowed to incubate for 2 hours in a humidified incubator at 37 °C. During this time dehydrogenases in viable cells reduces WST-8 tetrazolium to formazan, which will be detected by measuring the absorbance at 450 nm. Absorbance was measured by using a Tecan Infinite 200 Pro microplate reader. Three experiments were performed in triplicates per hydrogel candidate (n = 3).

3 | RESULTS AND DISCUSSION

3.1 | ECM mimic design and preparation

The studied hFF03 and its variants originate from the fibril-forming homodimeric coiled coil peptide FF03, previously reported by our group.[13] It consists of 3.5 heptad repeats,[13] thus creating "sticky ends" at the *N*-terminus of the peptide to trigger fiber-assembly.[13,18] Leucine residues comprise the hydrophobic core (positions *a* and *d*) of the coiled-coil, whereas additional stabilization of the α-helical coiled-coil structure occurs by positively and negatively charged amino acids lysine and glutamic acid in positions *e* and *g*. Furthermore, *b* and *c* positions are occupied with alanine residues to shield the solvent-exposed domain of the peptide and induce weak hydrophobic interactions between helices, thus, promoting fiber formation.[30] Solvent-exposed position *f* of hFF03 is occupied by lysine to enable side-chain functionalization using amine chemistry. Instead of the commonly used Boc-protected lysine, a methyltrityl-protected (Mtt) lysine was placed in position 17 (Mtt). The Mtt-group can be selectively removed[33] to access the ε-NH_2 of lysine for functionalization or built-up of the RGD sequence, by orthogonal solid-phase peptide synthesis (SPPS). RGD sequence was chosen, as it is a well-known recognition motif that promotes adhesion of cells and is presented by fibronectin and collagen in native ECMs.[37,38]

For the conjugation with the carbohydrate ligand mannose, the ε-NH_2 of lysine 17 was converted into a carboxy-functionality by reaction with glutaric anhydride.[13] Activation of the newly obtained carboxylic acid at the lysine side chain on resin and coupling of amino-functionalized mannose yields the corresponding peptide-carbohydrate conjugate. The monosaccharide mannose was chosen to study the impact of a sugar moieties on the hydrogel formation of the peptide. Based on this strategy (see Figure S1), a peptide library containing the undecorated peptide scaffold hFF03, a RGD-functionalized hFF03-K17-RGD, and a mannose-functionalized hFF03-K17-Man were synthesized (see Table 1).

Pure peptide hydrogels of hFF03 and its variants, and hydrogel mixtures were prepared and studied using overall peptide contents of 0.15, 0.30, and 0.50 wt% in order to systematically investigate the effect of increasing peptide concentration on properties of the respective hydrogels.

Twelve out of 18 compositions (see Table S1) immediately formed self-supporting gels within an incubation time of 30 minutes. Initial hydrogel formation was tested by inverting the sample vials for 30 minutes at room temperature (inversion test). This simple test is commonly used to evaluate gel formation of peptides.[30,39] Inversion test was also performed at 37 °C and showed no melting effects for all peptide hydrogel mixtures. In addition, mixtures consisting of hFF03 and 1% of hFF03-K17-Man, hFF03 and 5% of hFF03-K17-RGD, and a combination of both (hFF03 + 1% hFF03-K17-Man +5% hFF03-K17-RGD) were studied in terms of peptide structure and respective hydrogel formation. The latter mixture was chosen as this composition is close to the content of mannose and RGD in native ECMs.

3.2 | Analysis of peptide structure and scaffold formation

3.2.1 | Circular dichroism

hFF03 and its functionalized variants and mixtures show CD-spectra characteristic for an α-helical secondary structure with typical ellipticity minima around 208 nm and 222 nm as well as an ellipticity maximum at 195 nm with minimal differences between the studied samples (see Figure 2). For all samples, the ellipticity minimum around 222 nm is of higher intensity than the minimum around 208 nm indicating the formation of higher ordered structures.[40] The intensities of CD spectra subsides in the order hFF03, hFF03 + 1% hFF03-K17-Man, hFF03 + 5% hFF03-K17-RGD, hFF03 + 1% hFF03-K17-Man +5% hFF03-K17-RGD, hFF03-K17-Man, hFF03-K17-RGD, which indicates disturbed fiber formation due to the incorporation of RGD and mannose ligands as was also previously discussed for modified variants of the peptide scaffold FF03 (Figure 3).[13]

3.2.2 | Cryo TEM

The morphology of the peptide hydrogels was determined at peptide contents of 0.15 wt%, as density of peptide fibers would

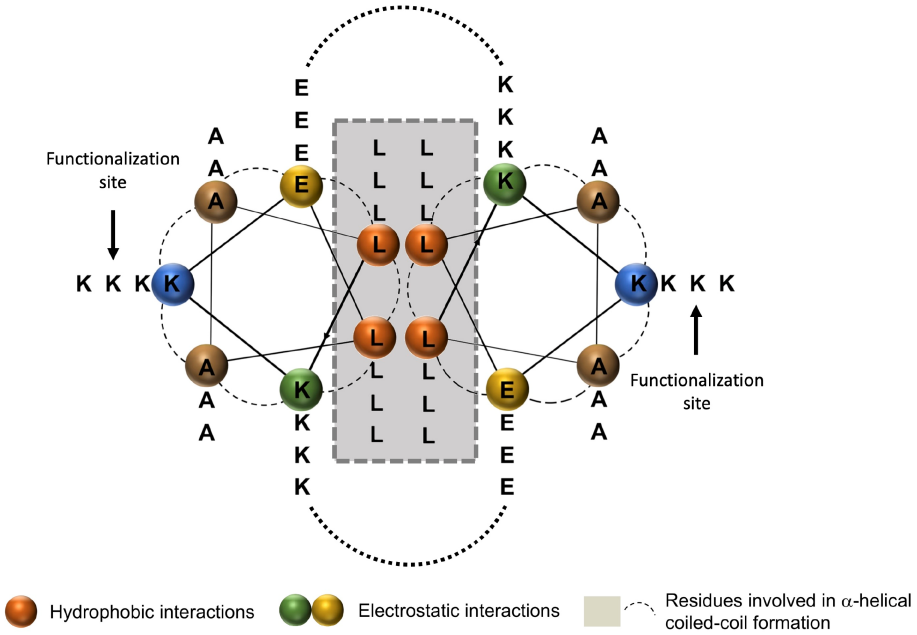

FIGURE 2 Helical wheel projection of peptide scaffold hFF03. Orange residues provide hydrophobic interaction, green and yellow residues provide electrostatic interaction. Remaining residues (brown and blue) are solvent exposed[32]

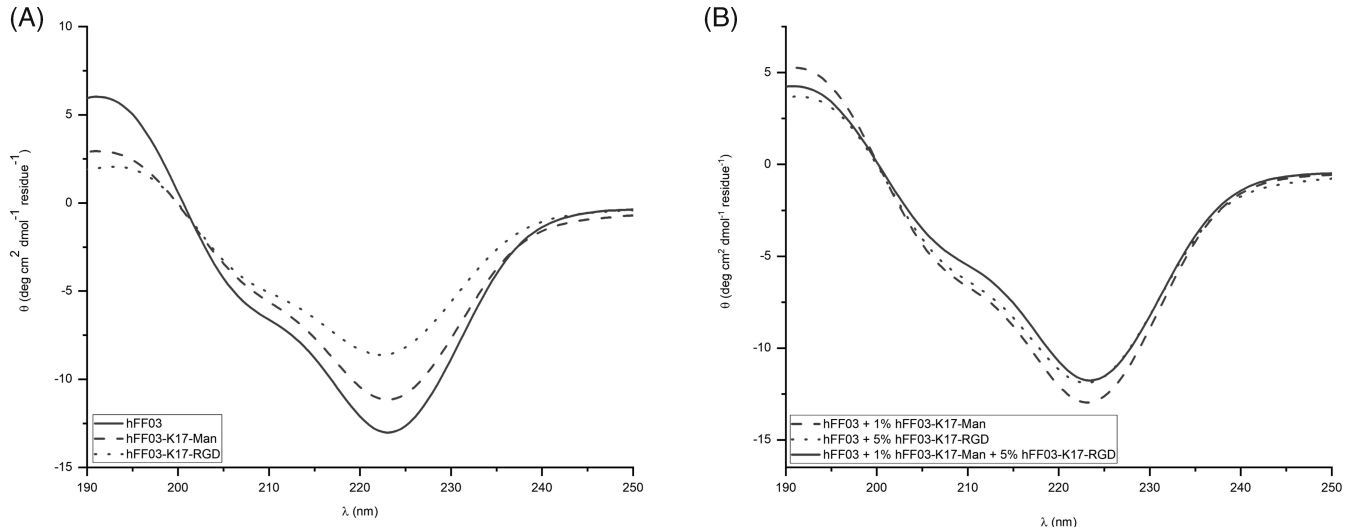

FIGURE 3 Circular dichroism (CD)-spectra of 0.5 wt% peptide hydrogels directly after sample preparation at 37 °C. A, pure peptide hydrogels and B, peptide hydrogel mixtures

otherwise be too high to obtain reasonable micrographs. Cryo-TEM micrographs show that all three hydrogels consist of a homogenous network of extended peptide fiber bundles with a diameter of 3 nm. Additionally, in the tested hydrogel mixture composed of hFF03 + 1% hFF03-K17-Man +5% hFF03-K17-RGD vesicular inclusions are found within the network structure of the hydrogel. These inclusions might result from hetero-assembled peptide fibers as cryo-TEM of the pure functionalized peptide hydrogels hFF03-K17-Man and hFF03-K17-RGD showed no vesicular inclusions over their whole three-dimensional structure (Figure 4).

3.2.3 | Rheological characterization

In order to compare the stiffness, respectively, the elastic and viscous properties of the hydrogels, which are the critical parameters within the context of biological or medical application, the pure peptide samples (with and without decoration by peptide or carbohydrate ligand) as well as mixtures thereof were investigated by shear strain oscillatory rheology. To ensure that the frequency dependent measurements are done within the linear viscoelastic regime an amplitude sweep in the deformation mode was performed prior to each experiment (see Figure S2 and Table S1), yielding the amplitude to be fixed

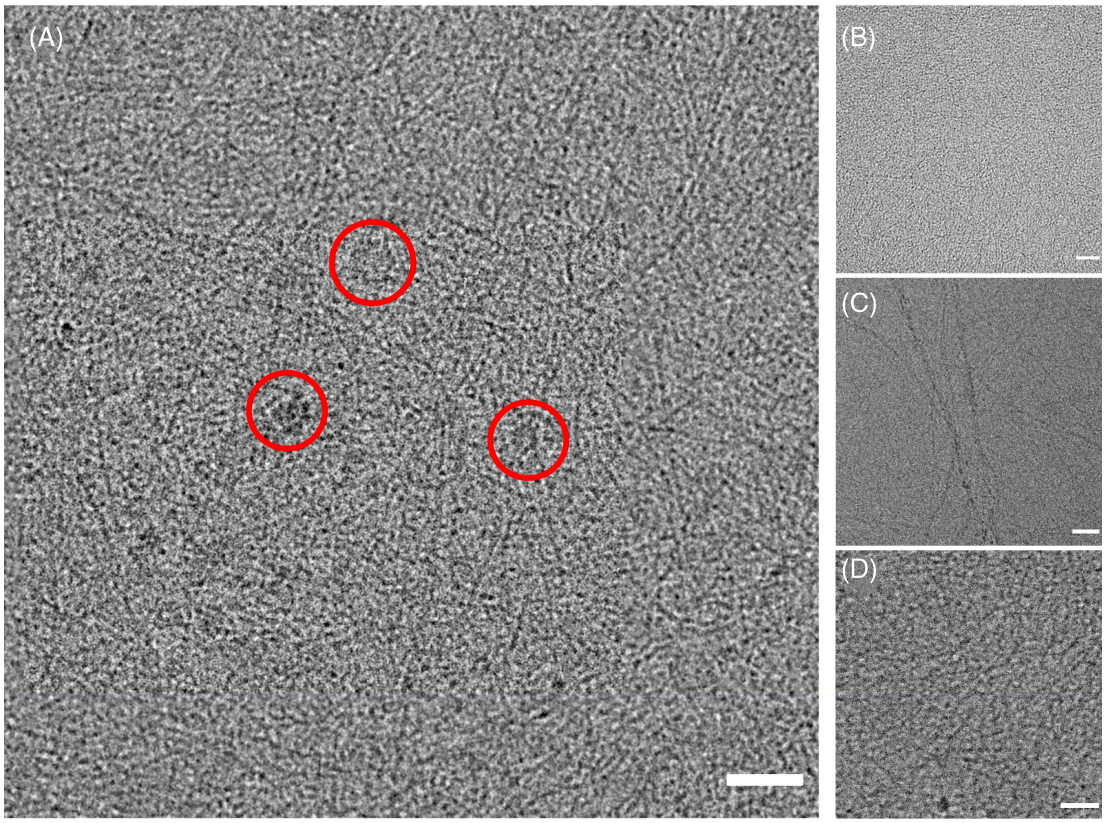

FIGURE 4 Cryo-transmission electron microscopy (Cryo-TEM) images of 0.15 wt% peptide hydrogels. A, hFF03 + 1% hFF03-K17-Man +5% hFF03-K17-RGD; B, hFF03; C, hFF03-K17-Man; D, hFF03-K17-RGD. Vesicular inclusions are marked by red circles. The scale bar denotes 50 nm

at a deformation of 2% for all experiments. From the subsequent frequency sweeps in the range of 0.05 to 20 Hz it was possible to determine the storage and loss moduli, G' and G", reflecting the elastic and viscous properties, respectively. The corresponding data sets for the hFF03 and decorated analogues are presented in Figure 5A,B and the data for the mixed peptide systems are presented in Figure 5C,D.

For all systems studied the elastic part, described by the G', is one decade larger than the viscous part, described by G", and this difference becomes larger with increasing concentration and at low frequencies. Both moduli are rather constant, in general just increasing somewhat with frequency, and only G" increases more strongly at higher frequency, indicating that here a mechanism for a more pronounced dissipation of mechanical energy becomes effective. The rather constant moduli indicate that in general these are gel-like systems. However, all samples are flowing very slowly (within 24 hours) when turned upside down within their container, thereby demonstrating their finite structural relaxation time or at least a yield stress lower than that exerted by gravitation. A very interesting observation here is, that the elastic and viscous properties of the systems increase with rising temperature, whereas normally the opposite trend is observed. However, the strength of the gel in terms of the critical deformation that can be exerted to it is lower at higher temperature (Figure 5). This indicates that here complex mechanisms determining the mechanical properties must be present by which the moduli increase with increasing temperature, but this more elastic gel then can sustain only a smaller deformation, changes that must be related to molecular reorganizations as a function of temperature.

To further characterize the frequency-dependent properties of the system the phase angle $\delta(\omega)$ (loss factor) defined as:

$$\tan(\delta(\omega)) = \frac{G''(\omega)}{G'(\omega)} \quad (1)$$

is a good reference to classify the gels.

The phase angles of hFF03 and hFF03 + 1%hFF03-K17-Man +5%hFF03-K17-RGD are exemplarily shown in Figure 6A,B for a temperature of 37 °C, which is the relevant temperature in the context of medical and biological applications (a comparison to data recorded at 25 °C is given in Figure S3). It is found that the phase angle is small for frequencies below 1 Hz, thereby quantifying the dominance of the elastic properties. Above 1 Hz it increases with increasing frequency, showing that here then the viscous properties of the gels become more prominent.[41,42] Further, as a function of concentration a smaller phase angle is observed, which indicates more pronounced elastic properties at higher concentrations.

Usually, the Kelvin-Voigt model is a good candidate to describe the frequency dependent moduli G' and G" of viscoelastic or gel-like materials, where the storage modulus G' is a constant (and related to

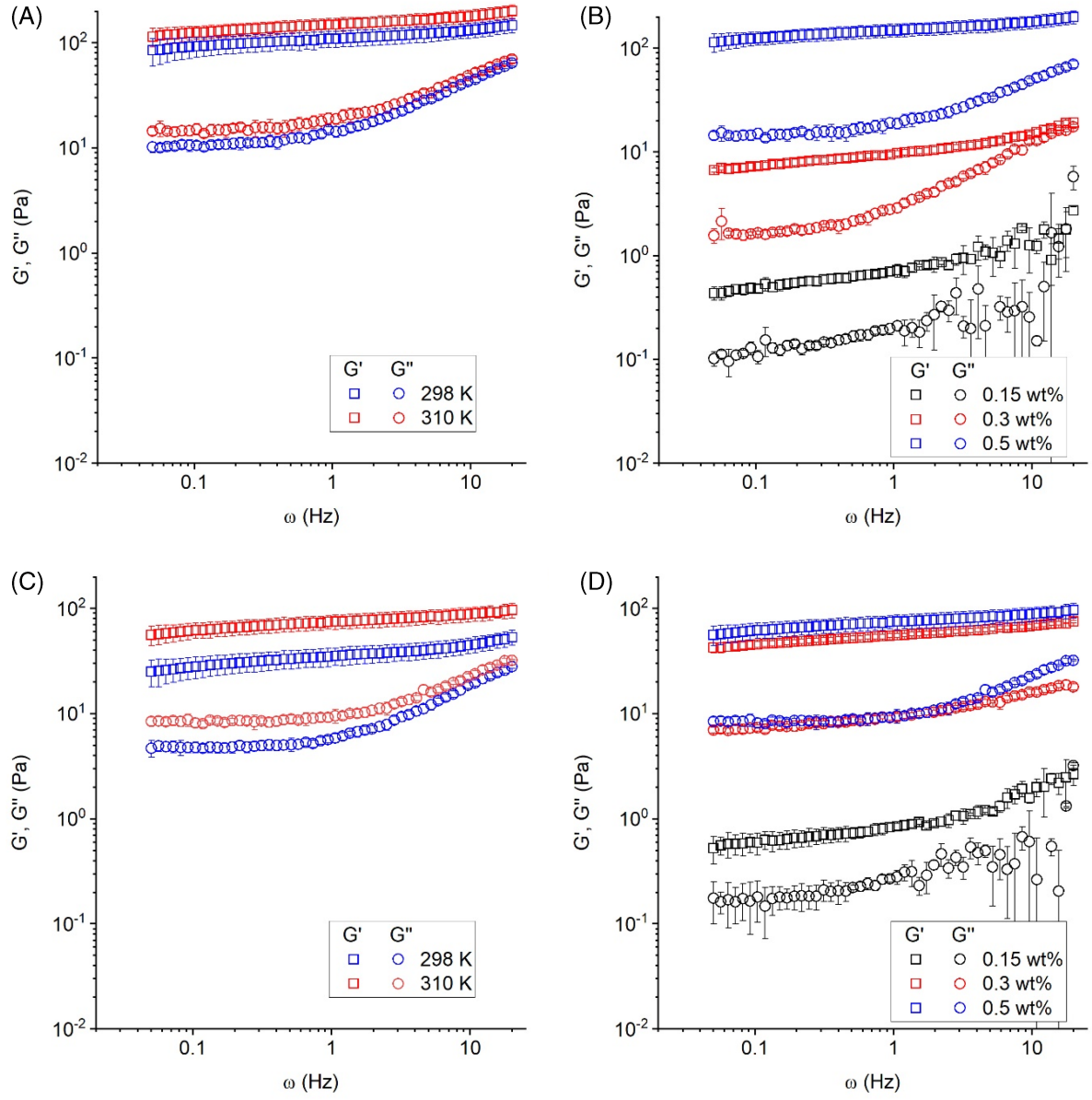

FIGURE 5 Moduli G' and G" of hFF03 for A, 25 and 37 °C at 0.5 wt%, and B, at 37 °C for different concentrations, and analogous of hFF03 + 1% hFF03-K17-Man +5% hFF03-K17-RGD for C, 25 and 37 °C at 0.5 wt%, and D, at 37 °C for different concentrations

the plateau modulus) and G" is linearly depending on the frequency with the viscosity of the material being the corresponding proportionality constant.[42] However, for the system under investigation this approximation is not suitable to describe the data, because neither G' is really constant nor is G" purely linearly depending on the frequency. Due to this fact, the so-called fractional Kelvin-Voigt model is employed. Within this model the moduli are described as follows.

$$G'(\omega) = E\,\omega^{\alpha}\cos\left(\frac{\pi\alpha}{2}\right) + G_0$$
$$G''(\omega) = E\,\omega^{\alpha}\sin\left(\frac{\pi\alpha}{2}\right) \qquad (2)$$

Details for the derivation of these quantities are given elsewhere.[42,43] In Equation (2) E is a fractional viscosity in units Pa s^{α} depending on the fractional exponent α ($0 < \alpha < 1$) and G_0 is the static load, equivalent to the plateau modulus (in the high frequency limit). Using this description, it is possible to model *G'* in an appropriate manner for the whole frequency range, while for *G"* the approximation works only in the high frequency regime, which might be attributed to inertia effects at low frequencies. The static load G_0 can be used to given an estimate for the crosslinking number density N_C and the corresponding average mesh size ξ through.[44]

$$N_C = \frac{G_0}{kT} = \frac{1}{\xi^3} \qquad (3)$$

where *k* is the Boltzmann constant and *T* is the absolute temperature. The results for ξ are tabulated in Table 2 for both investigated temperatures.

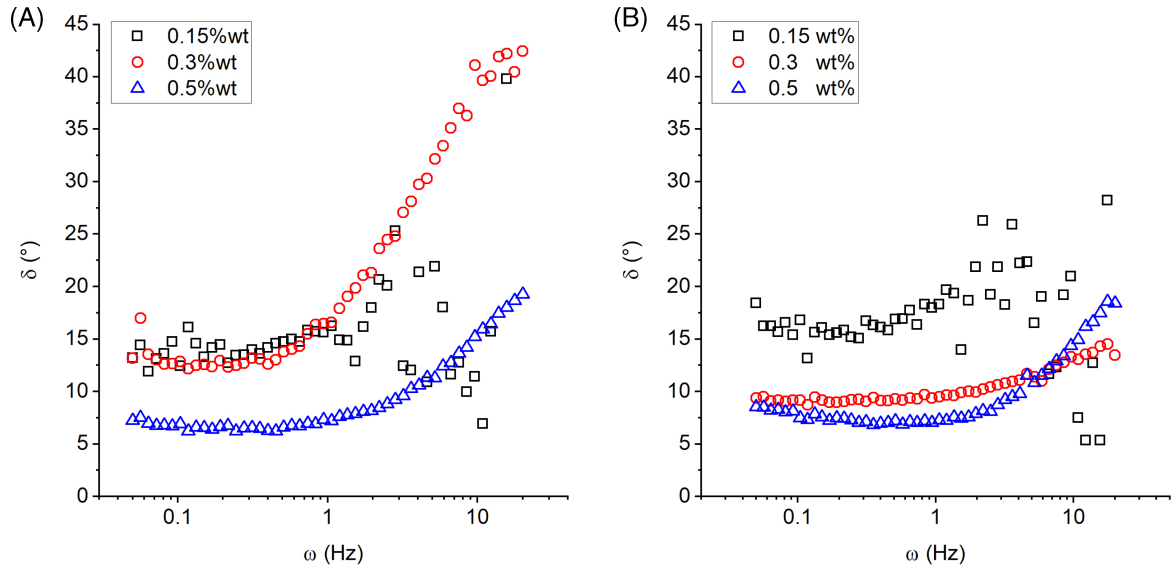

FIGURE 6 Phase angle at 37 °C of A, hFF03 and B, hFF03 + 1%hFF03-K17-Man +5%hFF03-K17-RGD at different concentrations

TABLE 2 Average mesh size ξ and static load G_0 as determined from fitting the data presented in Figure 5B,D by the expressions for moduli given in Equation (2), which are derived from the fractional Kelvin-Voigt model

Name	*c* (wt%)	G_1 (Pa)	ξ_1 (nm)	G_2 (Pa)	ξ_2 (nm)
hFF03	0.15	0.29	242.0	0.45	211.7
	0.30	3.65	104.0	6.00	89.3
	0.50	95.20	35.1	57.24	42.1
hFF03-K17-Man	0.15	2.66	115.6	6.08	88.9
	0.30	0.94	163.8	4.32	99.7
	0.50	6.03	88.0	15.28	65.4
hFF03-K17-RGD	0.15	1.63	136.3	1.33	147.7
	0.30	8.78	77.7	15.15	65.6
	0.50	37.55	47.8	39.09	47.8
hFF03 + 1% hFF03-K17-Man	0.15	0.27	246.9	0.33	235.5
	0.30	8.23	79.3	20.17	59.6
	0.50	22.44	56.8	19.42	60.4
hFF03 + 5% hFF03-K17-RGD	0.15	1.67	135.2	2.39	121.4
	0.30	17.48	61.7	23.26	56.9
	0.50	24.21	55.4	32.11	51.1
hFF03 + 1%hFF03-K17-Man +5%hFF03-K17-RGD	0.15	0.17	290.7	0.60	192.2
	0.30	16.97	62.3	16.61	63.6
	0.50	32.27	50.3	39.68	47.6

Note: The indices refer to the corresponding temperature T_1 = 25 °C and T_2 = 37 °C, respectively. The measurements have been carried out at 200 μm.

Comparing the values for the mesh size ξ presented in Table 2, it is found that in general ξ is decreasing with increasing concentration *c*. This is expected, however, for simple rod-like fibers one would expect a scaling of $\xi \sim c^{-0.5}$, while here the experimental changes are much larger. This indicates that the effective strengthening of the polypeptide works in a much more effective way than by the simple increase of overlapping junctions of the polymer chains. Further, it is notable that the mesh sizes at both temperatures, 25 °C and 37 °C, are of the same order of magnitude and follow the same trends.

3.2.4 | Small angle neutron scattering

In order to get a more detailed insight into the structural organization of hFF03 and its decorated analogues (hFF03-K17-Man and hFF03-K17-RGD) on a mesoscopic level, SANS measurements were performed for different peptide concentrations (0.15, 0.3 and 0.5 wt%). Further, mixtures of the pure and the decorated peptides were investigated. The scattering patterns for hFF03 without decoration and hFF03 + 1%hFF03-K17-Man +5%hFF03-K17-RGD as

function of the concentration are shown in Figure 7A,B, respectively.

Comparing the intensities of the scattering data presented in Figure 7, a well-defined concentration trend can be observed. That is, the intensity is increasing with increasing concentration for the investigated q-range. A direct comparison of scattering intensities of peptide hydrogels grouped by the three concentrations as shown in Figures S9 and S10 yields no difference between pure and decorated peptides. Hence, in the range of 1 to 50 nm their overall network structure must be very similar.

For all scattering patterns at intermediate q values an intensity scaling of q^{-1} can be taken as an indication for the formation of local rod-like structures.[45] In the lower q range the slope then increases substantially, following a power law of $\sim q^{-3}$ at lowest q, a behavior quite typically seen for the network structure of hydrogels.[46,47] The cross-over between the two power laws is indicative of the length of the local rod-like structure of the peptide chains. Such a structural arrangement is usually characterized by the persistence length L_p and the cross-sectional radius R_{cs}. In order to determine the latter one, the scattering data in the intermediate q regime were approximated by a modified Guinier approximation,[48,49] given by.

$$I(q) = \frac{A}{q} \cdot \exp\left(-\frac{q^2 R_{g,m}^2}{2}\right) \text{ with } R_{g,m}^2 = \frac{R_{cs}^2}{2} \quad (4)$$

In Equation (4) the pre-factor A on the right-hand side of the equation denotes the forward scattering intensity per unit length. R_{cs} is always in the range of 0.7 to 1.3 nm^{-1} (Table 3) and reflects the effective thickness of a bundle of peptide chains. The quantitative analysis described in the SI shows that these bundles correspond to 10 to 20 peptide chains (N_{pep}, Table S4). R_{cs} is generally decreasing with increasing concentration, which signifies that the chains are more stretched for the more dilute case, something to be expected in order to form a space-filling network. Comparing the cross-sectional radii obtained from fitting the intermediate q regime with Equation (4) the values are in good agreement with the results from TEM as presented in Figure 4 .

For a more accurate description of the scattering data, the intensities are approximated by a form factor model based on the flexible cylinder model as implemented in SasView.[50] This model originates from simulations done by Pedersen and Schurtenberger on semiflexible polymers, which take into account, excluded volume effects.[45] The scattering length density of the peptides is assumed to be 3.0×10^{10} cm^{-2}.[51] Comparing the cross-sectional radii obtained from the modified Guinier approximation and the Pedersen-Schurtenberger model, they are found to be in good agreement. Further, it is notable that the persistence length of the peptides is for all samples in the same order of magnitude and is around 8-14 nm. Assuming the peptide chains to be fully stretched they are found to be on average 17.2 nm, which is in good agreement with the determined persistence length. Further, the persistence length is also determined from a Kratky-plot (see exemplary Figure S5) yielding values around 15 nm (Table S3) and therefore confirming this observation. This means that the peptide chains are rather stretched and cylindrical in these network structures.

3.2.5 | Cytotoxicity of peptide hydrogels

hFF03 and its variants were studied as 3D-cell culture substrates and their cytotoxicity was assessed. To enhance biocompatibility of the studied peptides TFA counterions, inevitably added during peptide resin cleavage and subsequent purification by HPLC (eluents containing 0.1% TFA), were exchanged for chloride ions by treatment of

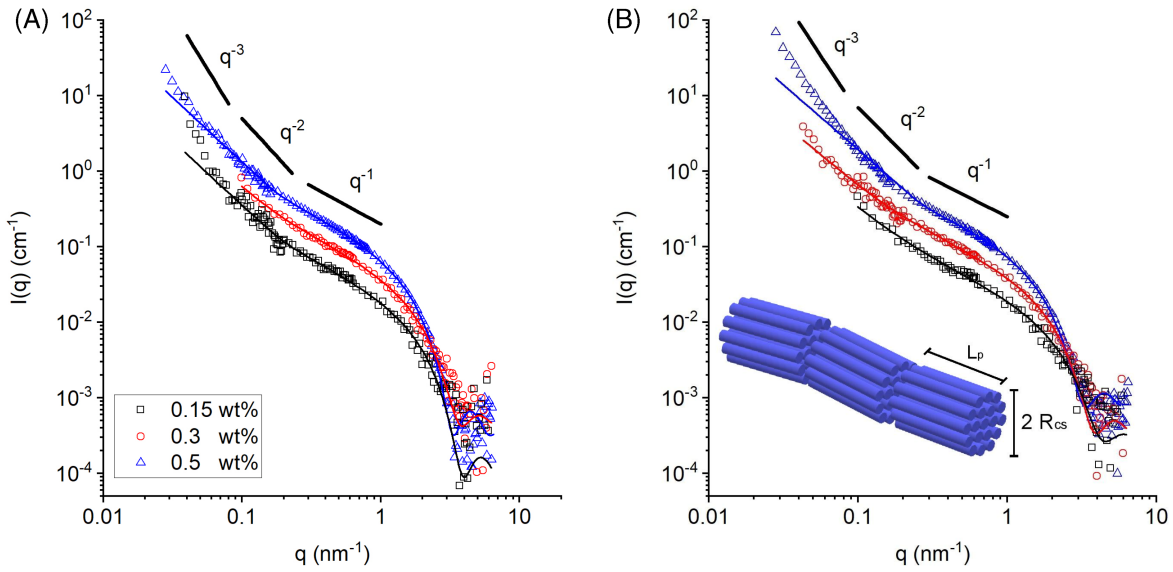

FIGURE 7 Scattering patterns of A, hFF03 and B, hFF03 + 1%hFF03-K17-Man +5%hFF03-K17-RGD at 0.15 (black), 0.3 (red) and 0.5 wt% (blue). The solid lines represent fits with a form factor model for flexible cylinders as suggested by Pedersen and Schurtenberger.[45] The temperature for all experiments was kept at 25 °C

TABLE 3 Fit results for the cross-sectional radius R_{cs} obtained from applying Equation (4) to the scattering data, and for persistence length and cross-sectional radius obtained by fitting the data with the Pedersen-Schurtenberger model for flexible, rod-like structures[45]

Name	c (wt%)	R_{cs} (nm)	L_p (nm)	R_{cs} (nm)
hFF03	0.5	1.30	9.81	1.14
	0.3	1.04	13.54	0.99
	0.15	1.01	9.20	0.96
hFF03-K17-Man	0.5	1.24	7.49	1.18
	0.3	1.18	8.94	1.09
	0.15	1.05	8.42	1.01
hFF03-K17-RGD	0.5	1.11	8.95	1.02
	0.3	1.30	9.96	1.09
	0.15	0.74	10.41	1.01
hFF03 + 1% hFF03-K17-Man	0.5	1.16	9.10	1.14
	0.3	0.78	12.68	0.79
	0.15	0.94	10.44	0.86
hFF03 + 5% hFF03-K17-RGD	0.5	1.16	6.96	1.14
	0.3	0.99	14.15	0.96
	0.15	1.03	9.80	0.98
hFF03 + 1% hFF03-K17-Man +5% hFF03-K17-RGD	0.5	1.16	6.59	1.14
	0.3	1.03	12.27	0.97
	0.15	0.91	10.70	0.84

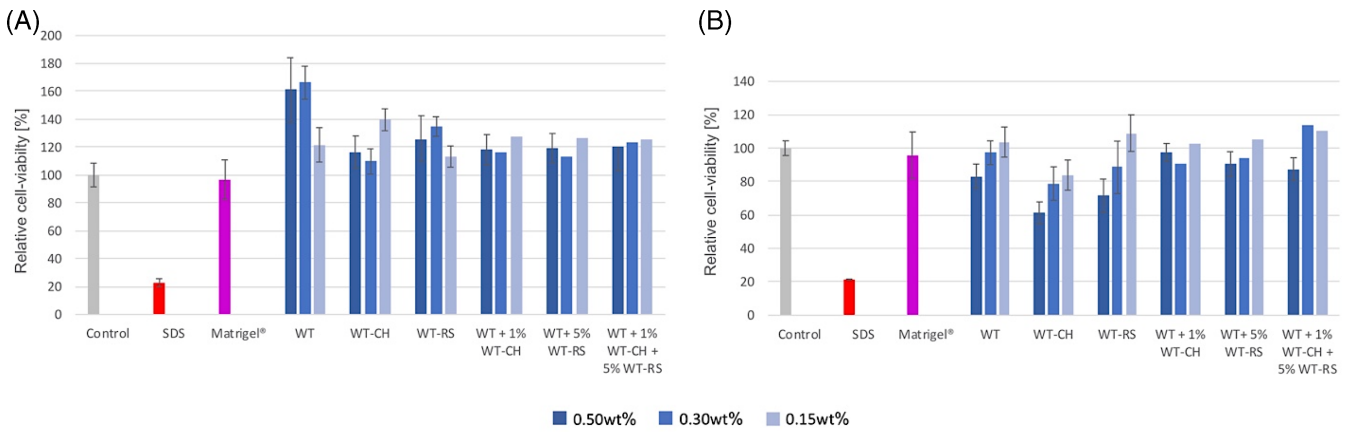

FIGURE 8 Viability profiles of seeded NIH3T3-cells on peptide hydrogels after A, 24 hours and B, 72 hours. WT: hFF03, WT-CH: hFF03-K17-Man, WT-RS: hFF03-K17-RGD. Error bars were calculated from triplicate determinations

the respective peptides with diluted HCl according to established protocols.[34]

Various hydrogel candidates were studied in a three-day cell culture by culturing embryonic mouse fibroblast cell line NIH/3T3 on hydrogel candidates, to assess optimal peptide content and compositions for cell growth (Figure 8). Cytotoxicity was determined relative to control standards, including pure medium, Matrigel and SDS. The commercially available and commonly used 3D cell culture scaffold Matrigel, which represents a mixture of different ECM proteins of the Engelbreth-Holm-Swarm mouse sarcoma, was used as negative control to compare viability of seeded cells on a 3D substrate. SDS was used to establish controlled cell death as positive control.

An increased viability of seeded cells was observed for all tested hydrogels candidates after 24 hours (Figure 8A). Compared to both controls (Medium and SDS), NIH/3T3 cells cultured on peptide hydrogels show a generally increased viability after 24 hours. Especially the undecorated hFF03 hydrogel at 0.3 wt% was tolerated most by the cells resulting in viability values higher than 160%, compared to the control. Cells cultured on each peptide hydrogel mixture showed viabilities in the same range with variations up to 10%. After 72 hours, relative cell-viability of cells cultured on 0.5 wt% hFF03-K17-Man hydrogels decreased to 60% (Figure 8B). Whereas the other two hydrogels containing 0.5 wt% peptide show profiles ranging from 70% to 97% relative viability compared to the control. Also, for all 0.3 wt% hydrogels average viabilities between 94% and 78% were

determined after 72 hours. Strikingly, except for hFF03-K17-Man, all 0.15 wt% candidates show cell-viability profiles above 100% relative to both controls. The results show, on the one hand, that the newly designed coiled-coil-based peptide hydrogels are suitable cell-culture matrices; and on the other hand, that only small differences in matrix composition with regard to peptide content and presented ligand density have a great effect on cell-viability. Fine-tuning these parameters, and thus overall chemical and physical properties of the resulting hydrogels, presents a pivotal point in the design of artificial ECM. Within the presented system fine-tuning is readily performed by varying the concentrations of functionalized coiled-coil monomers peptides. Hence, the presented approach enables an efficient methodology to access tailored biomaterials for the applications in cell culture experiments with optimized composition.

4 | CONCLUSION

Herein, we report the development of a homomeric coiled coil-based peptide (hFF03) that forms self-supporting hydrogels and functions as a potent cell-culture matrix. Using an all-on-solid-phase-synthesis approach, hFF03 was functionalized with peptide sequence RGD or carbohydrate mannose to include biologically relevant ligands. Utilizing the modularity of the coiled-coil design, hFF03 and its functionalized variants were mixed to obtain hydrogels that comprise defined ratios of RGD or mannose ligands that are distributed and multivalently presented throughout the 3D-structure of the hydrogel. This approach allows for fine-tuning of concentration of functional ligands, thus, fine-tuning of physicochemical properties of the resulting artificial ECM. These new 3D constructs were studied regarding their structural and mechanical properties as well as cytotoxicity. Cryo-TEM and neutron scattering experiments revealed fibrillar networks with rather stiff and stretched fibrillar chains, characterized by persistence lengths of 10 to 15 nm and they are composed of about 10 to 20 parallel peptide chains. Further Cryo-TEM experiments on different mixtures of that is, hFF03-K17-Man and hFF03-K17-RGD would be promising to study the structural properties of the system. Oscillatory rheology showed that these networks respond mainly elastic and the storage modulus increases very strongly with rising peptide concentration. Interestingly, the elastic properties do not decrease with increasing temperature but even become somewhat larger. Initial cytotoxicity assays using NIH/3T3 cells showed an improved viability of seeded cell populations on hFF03-based peptide hydrogels. Compared to other ex vivo materials, the herein presented system has the advantage of being easily accessible by chemical synthesis, without significant batch-to-batch variation. Moreover, the herein described methodology enables the development of peptide hydrogels that are tunable with regard to composition and density of presented ligands, which are important factors in systematic approaches that correlate hydrogel nature and properties with directing cellular behavior like proliferation and differentiation. Further studies on cell viability and cellular attachment via RGD-sequence of multiple cell types like stem cells and evaluation on possible applications of the here described 3D materials in tissue engineering and stem cell differentiation are in progress.

ACKNOWLEDGMENTS

The authors acknowledge financial support by the DFG-CRC 765 "Multivalency" (SFB 765/2-2014). Further, the authors thank the Laboratoire Léon Brillouin (Saclay, France) as well as the Helmholtz Zentrum Berlin (Berlin, Germany) for granting the neutron scattering beamtime at PAXY, respectively, V4 spectrometer. The authors are grateful to Prof. Marie Weinhart for providing NIH/3T3 cells. Open access funding enabled and organized by Projekt DEAL.

CONFLICT OF INTEREST

The authors declare no competing interest.

AUTHOR CONTRIBUTIONS

The manuscript was written through contributions of all authors. Beate Koksch and Michael Gradzielski initiated this study. Katharina S. Hellmund performed synthesis and purification of hFF03, hFF03-K17-Man and hFF03-K17-RGD, circular dichroism experiments, cell culture and cytotoxity testings. Benjamin von Lospichl performed rheological and SANS experiments. Christoph Böttcher and Kai Ludwig performed cryo-TEM measurements. Uwe Keiderling and Laurence Noirez supported SANS experiments. Annika Weiß assisted synthesis and purification of peptides and circular dichroism experiments. Beate Koksch, Michael Gradzielski, Katharina S. Hellmund and Benjamin von Lospichl wrote the manuscript with assistance from Dorian J. Mikolajczak. All authors have given approval to the final version of the manuscript. Katharina S. Hellmund and Benjamin von Lospichl contributed equally.

DATA AVAILABILITY STATEMENT

The data that supports the findings of this study are available in the supplementary material of this article.

ORCID

Beate Koksch https://orcid.org/0000-0002-9747-0740

REFERENCES

[1] C. S. Hughes, L. M. Postovit, G. A. Lajoie, *Proteomics* **2010**, *10*, 1886.
[2] C. Lin, M. J. Bissell, *FASEB J.* **1993**, *7*, 737.
[3] G. R. Martin, H. K. Kleinman, *Hepatology* **1981**, *1*, 264.
[4] H. K. Kleinman, J. Graf, Y. Iwamoto, G. T. Kitten, R. C. Ogel, M. Sasaki, Y. Yamada, G. R. Martin, L. Luckenbill-Edds, *Ann. N. Y. Acad. Sci.* **1987**, *513*, 134.
[5] H. K. Kleinman, R. J. Klebe, G. R. Martin, *J. Cell Biol.* **1981**, *88*, 473.
[6] H. Geckil, F. Xu, X. Zhang, S. Moon, U. Demirci, *Nanomedicine* **2010**, *5*, 469.
[7] N. Blow, *Nat. Methods* **2009**, *6*, 619.
[8] H. K. Kleinman, M. L. McGarvey, L. A. Liotta, P. G. Robey, K. Tryggvason, G. R. Martin, *Biochemistry* **1982**, *21*, 6188.
[9] H. K. Kleinman, G. R. Martin, *Cancer Biol.* **2005**, *15*, 378.
[10] M. W. Tibbitt, K. S. Anseth, *Biotechnol. Bioeng.* **2009**, *103*, 655.
[11] E. H. Nguyen, W. T. Daly, N. N. T. Le, M. Farnoodian, D. G. Belair, M. P. Schwartz, C. S. Lebakken, G. E. Ananiev, M. A. Saghiri, T. B. Knudsen, N. Sheibani, W. L. Murphy, *Nat. Biomed. Eng.* **2017**, *1*, 96.

[12] S. Lou, X. Wang, Z. Yu, L. Shi, *Adv. Sci.* **2019**, *6*, 1802043.
[13] E. Zacco, C. Anish, C. E. Martin, H. Berlepsch, E. Brandenburg, P. H. Seeberger, B. A. Koksch, *Biomacromolecules* **2015**, *16*, 2188.
[14] E. Zacco, J. Hütter, J. L. Heier, J. Mortier, P. H. Seeberger, B. Lepenies, B. Koksch, *ACS Chem. Biol.* **2015**, *10*, 2065.
[15] K. S. Hellmund, B. Koksch, *Front. Chem.* **2019**, *7*, 172.
[16] D. N. Woolfson, *Adv. Protein Chem.* **2005**, *70*, 79.
[17] J. A. Falenski, U. I. M. Gerling, B. Koksch, *Bioorg. Med. Chem.* **2010**, *18*, 3703.
[18] K. Pagel, B. Koksch, *Curr. Opin. Chem. Biol.* **2008**, *12*, 730.
[19] K. Pagel, S. C. Wagner, R. R. Araghi, H. Von Berlepsch, C. Böttcher, B. Koksch, *Chemistry* **2008**, *14*, 11442.
[20] A. N. Lupas, M. Gruber, *Adv. Protein Chem.* **2005**, *70*, 37.
[21] R. S. Hodges, *Biochem. Cell Biol.* **1996**, *74*, 133.
[22] J. R. Litowski, R. S. Hodges, *J. Biol. Chem.* **2002**, *277*, 37272.
[23] P. B. Harbury, T. Zhang, P. S. Kim, T. A. Alber, *Science* **1993**, *262*, 1401.
[24] J. M. Fletcher, A. L. Boyle, M. Bruning, S. J. Bartlett, T. L. Vincent, N. R. Zaccai, C. T. Armstrong, E. H. C. Bromley, P. J. Booth, R. L. Brady, A. R. Thomson, D. N. Woolfson, *ACS Synth. Biol.* **2012**, *1*, 240.
[25] E. Wolf, P. S. Kim, B. Berger, *Protein Sci.* **1997**, *6*, 1179.
[26] E. F. Banwell, E. S. Abelardo, D. J. Adams, M. A. Birchall, A. Corrigan, A. M. Donald, M. Kirkland, L. C. Serpell, M. F. Butler, D. N. Woolfson, *Nat. Mater.* **2009**, *8*, 596.
[27] N. Mehrban, E. Abelardo, A. Wasmuth, K. L. Hudson, L. M. Mullen, A. R. Thomson, M. A. Birchall, D. N. Woolfson, *Adv. Healthc. Mater.* **2014**, *3*, 1387.
[28] N. Mehrban, B. Zhu, F. Tamagnini, F. I. Young, A. Wasmuth, K. L. Hudson, A. R. Thomson, M. A. Birchall, A. D. Randall, B. Song, D. N. Woolfson, *ACS Biomater. Sci. Eng.* **2015**, *1*, 431.
[29] S. A. Potekhin, T. N. Melnik, V. Popov, N. F. Lanina, A. A. Vazina, P. Rigler, A. S. Verdini, G. Corradin, A. V. Kajava, *Chem. Biol.* **2001**, *8*, 1025.
[30] E. F. Banwell, E. S. Abelardo, D. J. Adams, M. A. Birchall, A. Corrigan, A. M. Donald, M. Kirkland, L. C. Serpell, M. F. Butler, D. N. Woolfson, *Nat. Mater.* **2009**, *8*, 596.
[31] M. D. Pierschbacher, E. Ruoslahti, *Proc. Natl. Acad. Sci. U. S. A.* **1984**, *81*, 5985.
[32] K. S. Hellmund, *Coiled-Coil Based 3D Scaffolds as Highly Specialized Biological Microenvironments*, Freie Universität Berlin, Berlin **2019**.
[33] Millipore, M. novabiochem (r) guide to selection of building blocks.
[34] V. V. Andrushchenko, H. J. Vogel, E. J. Prenner, *J. Pept. Sci.* **2007**, *13*, 37.
[35] U. Keiderling, *Appl. Phys. A* **2002**, *74*, 1455.
[36] A. Brûlet, D. Lairez, A. Lapp, J.-P. Cotton, *J. Appl. Crystallogr.* **2007**, *40*, 165.
[37] E. R. G. D. Ruoslahti, *Annu. Rev. Cell Dev. Biol.* **1996**, *12*, 697.
[38] C. Cha, W. B. Liechty, A. Khademhosseini, N. A. Peppas, *ACS Nano* **2012**, *6*, 9353.
[39] M. Lian, X. Chen, Y. Lu, W. Yang, *ACS Appl. Mater. Interfaces* **2016**, *8*, 25036.
[40] M. J. Pandya, G. M. Spooner, M. Sunde, J. R. Thorpe, A. Rodger, D. N. Woolfson, *Biochemistry* **2000**, *39*, 8728.
[41] R. L. Bagley, P. J. Torvik, *AIAA J.* **1983**, *21*, 741.
[42] L. B. Eldred, W. P. Baker, A. N. Palazotto, *AIAA J.* **1995**, *33*, 547.
[43] R. Lewandowski, B. Chorazyczewski, *Comput. Struct.* **2010**, *88*, 1.
[44] M. Doi, S. F. Edwards, *The Theory of Polymer Dynamics*, Oxford University Press, New York **1986**.
[45] J. S. Pedersen, P. Schurtenberger, *Macromolecules* **1996**, *29*, 7602.
[46] F. Horkay, P. J. Basser, A.-M. Hecht, E. Geissler, *Polymer* **2005**, *46*, 4242.
[47] M. Vamvakaki, C. S. Patrickios, P. Lindner, M. Gradzielski, *Langmuir* **2007**, *23*, 10433.
[48] R. P. Hjelm, P. Thiyagarajan, H. Alkan-Onyuksel, *J. Phys. Chem.* **1992**, *96*, 8653.
[49] R. P. Hjelm, C. Schteingart, A. F. Hoffmann, D. S. Sivia, *J. Phys. Chem.* **1995**, *99*, 16395.
[50] https://www.sasview.org/publications/.
[51] B. Jacrot, *Reports Prog. Phys.* **1976**, *39*, 911.

SUPPORTING INFORMATION

Additional supporting information may be found online in the Supporting Information section at the end of this article.

How to cite this article: Hellmund KS, von Lospichl B, Böttcher C, et al. Functionalized peptide hydrogels as tunable extracellular matrix mimics for biological applications. *Peptide Science*. 2021;113:e24201. https://doi.org/10.1002/pep2.24201